GA–A26264

DIII-D RESEARCH IN SUPPORT OF ITER

by
E.J. STRAIT and the DIII-D TEAM

SEPTEMBER 2008

DISCLAIMER

GA–A26264

DIII-D RESEARCH IN SUPPORT OF ITER

by
E.J. STRAIT and the DIII-D TEAM

This is a preprint of a paper to be presented at the 22nd IAEA Fusion Energy Conference, October 13-18, 2008, in Geneva, Switzerland, and to be published in the *Proceedings.*

Work supported in part by
the U.S. Department of Energy
under DE-FC02-04ER54698

GENERAL ATOMICS PROJECT 30200
SEPTEMBER 2008

DIII-D Research in Support of ITER

E.J. Strait and the DIII-D Team

General Atomics, San Diego, California, USA

e-mail contact of main author: strait@fusion.gat.com

Abstract. DIII-D research is providing key information for the design and operation of ITER. Discharges that simulate ITER operating scenarios in conventional H-mode, advanced inductive, hybrid, and steady state regimes have achieved normalized performance consistent with ITER's goals for fusion performance. Stationary discharges with high β_N and 90% noninductive current that project to Q=5 in ITER have been sustained for a current relaxation time (~2.5 s), and high-beta wall-stabilized discharges with fully non-inductive current drive have been sustained for more than one second. Detailed issues of plasma control have been addressed, including the development of a new large-bore startup scenario for ITER. A broad research program provides the physics basis for predicting the performance of ITER. Recent key results include the discovery that the L-H power threshold is reduced with low neutral beam torque, and the development of a successful model for prediction of the H-mode pedestal height in DIII-D. Research areas with the potential to improve ITER's performance include the demonstration of ELM-free "QH-mode" discharges with both co and counter-injection, and validation of the predicted torque generated by static, non-axisymmetric magnetic fields. New diagnostics provide detailed benchmarking of turbulent transport codes and direct measurements of the anomalous transport of fast ions by Alfvén instabilities. DIII-D research also contributes to the basis for reliable operation in ITER, through active control of the chief performance-limiting instabilities. Recently, ELM suppression with resonant magnetic perturbations has been demonstrated at collisionality similar to ITER's, while simultaneous stabilization of NTMs (by localized current drive) and RWMs (by magnetic feedback) has allowed stable operation at high beta and low rotation. In research aimed at improving the lifetime of material surfaces near the plasma, recent experiments have investigated several approaches to mitigation of disruptions, including injection of low-Z gas and low-Z pellets, and have shown the conditions that minimize core impurity accumulation during radiative divertor operation. Investigation of carbon erosion, transport, and co-deposition with hydrogenic species, and methods for the removal of co-deposits, will contribute to the physics basis for initial operation of ITER with a carbon divertor.

1. Introduction

DIII-D research is aimed at providing the physics basis to optimize the tokamak approach to fusion energy production, and much of the program directly supports the design and future operation of ITER. Recent DIII-D research has addressed specific, near-term issues for ITER such as design of new coils for suppression of edge-localized modes (ELMs) and specification of poloidal field systems for control of plasma shape and vertical stability. A longer term goal is to develop and characterize ITER-relevant operating scenarios that integrate high fusion performance, stable operation, and appropriate boundary conditions, ultimately simulating the entire discharge evolution (breakdown, ramp-up, flattop, and ramp-down). Recent experiments include discharges that demonstrate normalized performance consistent with ITER's Q=10 mission, and significant progress has been made toward scenarios with 100% noninductive current for the Q=5 steady-state goal. DIII-D also contributes to a broad scientific base for tokamak physics that will help to optimize fusion performance in ITER.

As summarized in this paper, DIII-D experiments that simulate several specific high-gain and steady-state scenarios envisioned for ITER provide a platform for projections of fusion performance and tests of plasma control (Sec. 2). Investigations of the fundamental physics of transport, stability, and wave-particle interactions contribute to the basis for prediction and improvement of ITER's performance (Sec. 3). Progress toward the understanding and active control of MHD instabilities is contributing to the basis for stable and reliable operation in ITER (Sec. 4). DIII-D research is also aimed at improving the lifetime of plasma-facing materials in fusion devices such as ITER by reducing peak heat flux and improving the

understanding of plasma-wall interactions, including hydrogenic fuel retention (Sec. 5). Future DIII-D research will continue to investigate these issues and to provide the basis for high-performance steady-state operation of ITER.

2. Integrated Scenario Development

ITER demonstration scenarios. A major objective of DIII-D research is the development of ITER-relevant operating scenarios that integrate high fusion performance, stable operation, and appropriate boundary conditions. This year, we have focused on evaluation of four operating scenarios for ITER, in discharges with the ITER aspect ratio and cross-section (Fig. 1) but scaled down in size [1]. These discharges allow a direct comparison, in a single device, of the fusion performance and operating characteristics of these scenarios. To date, the emphasis has been on reproducing global parameters such as discharge shape, safety factor, and normalized beta; future work will begin to address other dimensionless parameters such as collisionality and T_i/T_e. As summarized in Fig. 1, the cases studied include the conventional H-mode baseline scenario (Scenario 2), an advanced inductive scenario (aimed at the goal of Q=30 in ITER), the "hybrid" scenario (Scenario 3), and the steady-state scenario (Scenario 4). In all four cases, the fusion performance characterized by $G = \beta_N H_{89}/q_{95}^2$ reaches the level required for ITER's goals: fusion gain $Q \geq 10$ for the first three cases and Q=5 for the steady-state case. (Here $\beta_N = \beta(aB/I)$ is the normalized beta and H_{89} is energy confinement time normalized to the ITER89P L-mode scaling [2].) Recently, fusion performance consistent with Q>10 in ITER has also been demonstrated in advanced inductive discharges with low neutral beam torque, and hybrid mode operation has been shown to be compatible with ELM suppression [3]. High-beta wall-stabilized scenarios compatible with steady state operation have been sustained with a stationary current density profile for 2.5 s, or about one current relaxation time.

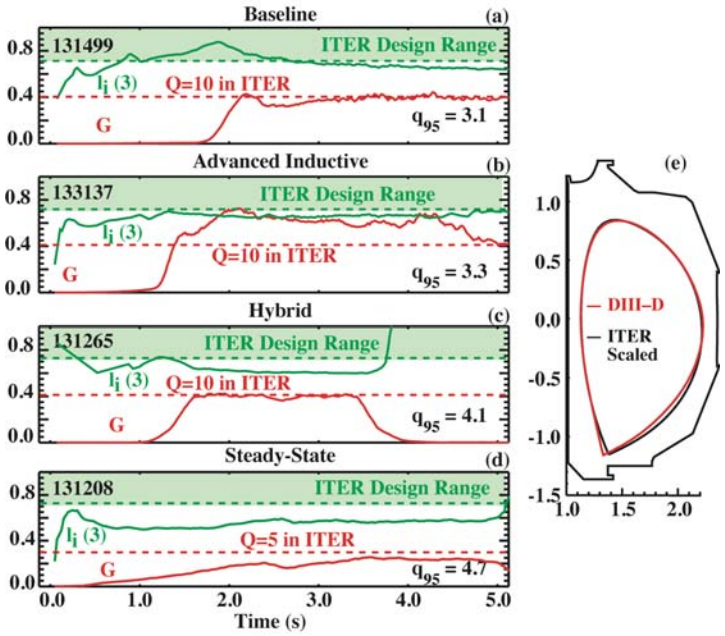

FIG. 1. ITER demonstration discharges characterized by $G = \beta_N H_{89}/q_{95}^2$ and internal inductance $l_i(3)$, for cases including (a) baseline scenario with q_{95}~3 and β_N~2, (b) advanced inductive scenario with q_{95}~3.3 and β_N~2.8, (c) hybrid scenario with q_{95}~4.1 and β_N~2.8, and (d) steady-state scenario with q_{95}~4.7 and β_N~2.8–3.0. Also shown is (e) the DIII-D discharge shape compared to the scaled-down ITER shape.

The small differences from the ITER shape seen in Fig. 1(e) are motivation for a study of the sensitivity of fusion performance to discharge shape; initial results indicate that the triangularity can influence performance through the stability of the H-mode pedestal. These discharges also displayed several issues known to be of concern for ITER, including large infrequent ELMs, and neoclassical tearing modes that lead to confinement degradation or disruption. Progress on solutions to these stability issues will be discussed further in Sec. 4.

Plasma startup and control. DIII-D discharges have also been used to study the detailed evolution and control of ITER discharges. As seen in Fig. 1, the internal inductance in the DIII-D discharges was found to lie at or below the lower limit of the ITER specification ($0.7 < l_i(3) < 1.0$), leading to recommendations for an increase in poloidal field coil current capabilities and a change in the divertor coil location. Experiments in DIII-D and other tokamaks have provided guidance [4] for vertical stability requirements in ITER: $\Delta Z_{max}/a$, the ratio of the maximum controllable vertical displacement to the minor radius, must be at least 5% for safe operation.

The "small-bore" scenario initially envisioned for startup of ITER plasmas was shown in DIII-D experiments to result in values of $l_i(3)$ larger than the ITER specification, with the potential for difficulties with vertical stability control. A new "large-bore" startup [5] was demonstrated on DIII-D (Fig. 2), in which the plasma goes to an X-point configuration early in the current ramp, reducing the heat load on the limiter and reducing the internal inductance. With the use of electron cyclotron heating at plasma initiation, this startup has proved robust with toroidal electric fields as low as 0.21 V/m (the ITER specification is 0.3 V/m) and smaller resistive flux consumption. Feedback control of internal inductance during the current ramp has been developed, using dI_p/dt as the actuator; this allows vertical stability limits to be avoided.

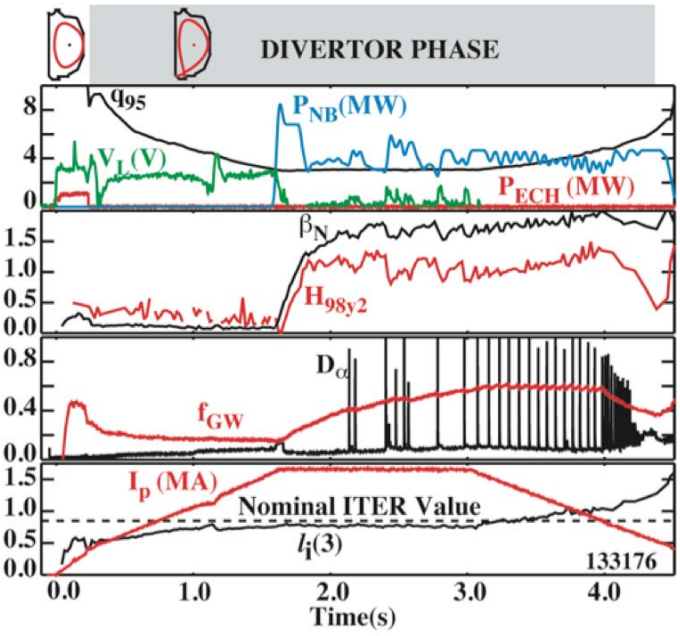

FIG. 2. ITER demonstration discharge with large-bore, low-voltage startup, showing (a) electron cyclotron heating power P_{ECH}, neutral beam power P_{NB}, one-turn loop voltage V_L, and safety factor q_{95}; (b) normalized beta β_N and normalized energy confinement H_{98y2}; (c) ratio f_{GW} of electron density to the Greenwald limit, and divertor D_α emission; (d) plasma current I_p and internal inductance $l_i(3)$. The discharge shape is shown at two times during the discharge, and shading indicates the duration of the X-point configuration.

Steady-state scenarios. Two approaches are being pursued at DIII-D toward steady-state, noninductive discharges [6] for ITER and devices beyond ITER. The first approach is a high q_{min}, wall-stabilized configuration at moderate β_N, similar to ITER's Scenario 4. Closed loop feedback control of the evolution of q_{min} during the plasma current ramp up and early flattop, using electron cyclotron heating to modify T_e, sets the value of q_{min} at the start of the high β_N phase. With over 3 MW of electron cyclotron current drive applied broadly at $q \lesssim 2$, neoclassical tearing modes were avoided (through current profile modification rather than direct stabilization) and discharges with $\beta_N \sim 3.5$ and fully noninductive current sustainment for more than one second were obtained (Fig. 3). The second approach aims to achieve high β_N without the need for wall stabilization, by operation at higher $l_i \sim 1.1$. Such discharges have reached $\beta_N = 5$ transiently, with noninductive current fraction greater than unity (up to 90% bootstrap current) and very good energy confinement (Fig. 4). In this example, active MHD spectroscopy shows a reduction in the stability of the n=1 kink mode at peak beta, suggesting that the discharge may approach or exceed the ideal MHD no-wall kink stability limits.

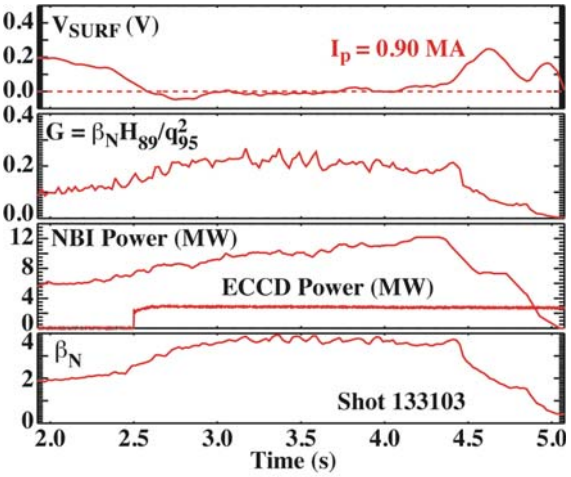

FIG. 3. Candidate for steady-state scenario, with $q_{min} \geq 1.5$ and $q_{95} \sim 6$, showing (a) surface loop voltage V_{SURF}; (b) fusion figure of merit $G = \beta_N H_{89} / q_{95}^2$; (c) neutral beam power P_{NBI} and electron cyclotron current drive power P_{ECCD}; and (d) normalized beta β_N.

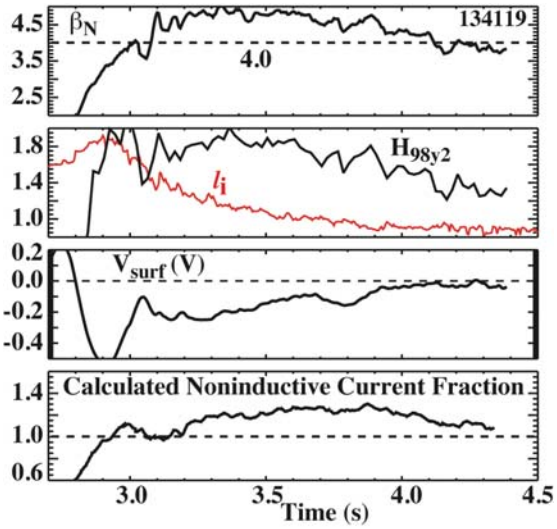

FIG. 4. High beta discharge at higher internal inductance, with $q_{min} \gtrsim 1$ and q_{95}~7–8, showing (a) normalized beta β_N; (b) normalized energy confinement H_{98y2} and internal inductance l_i; (c) surface loop voltage V_{surf}; and (d) calculated noninductive current fraction.

3. Prediction and Improvement of Fusion Performance

Investigations of the fundamental science of transport, stability, and wave-particle interactions contribute to the basis for prediction and improvement of ITER's performance. Recent DIII-D results include the investigation of energy transport and L-H power threshold in hydrogen plasmas, improved predictive capability for the H-mode pedestal, detailed benchmarking of gyrokinetic transport calculations against experimental data, progress in understanding and expanding the operating range of the ELM-free quiescent H-mode, improved understanding of plasma rotation in the absence of neutral beam torque, and progress in measuring and understanding fast ion transport due to Alfvénic instabilities.

Hydrogen plasmas. The ion mass dependence of H-mode performance and the L-H power threshold is of key importance to ITER, since the initial phase of ITER operation is planned to be with hydrogen and/or helium plasmas. A recent series of DIII-D experiments has shown that the L-H power threshold is reduced at low or negative torque, a potentially favorable result for ITER. In the DIII-D experiments, hydrogen was used for both fueling and neutral beam heating, yielding a measured hydrogen purity (relative to the residual deuterium) of more than 90%. The L-H power threshold in hydrogen plasmas was found to be roughly a factor of 2 larger than in deuterium (Fig. 5). However, the threshold in both H and D plasmas exhibits a strong dependence on the neutral beam torque [7], and the threshold in hydrogen plasmas with counter-injection was approximately the same as that of deuterium plasmas with strong co-injection. Comparison of hydrogen and deuterium discharges with

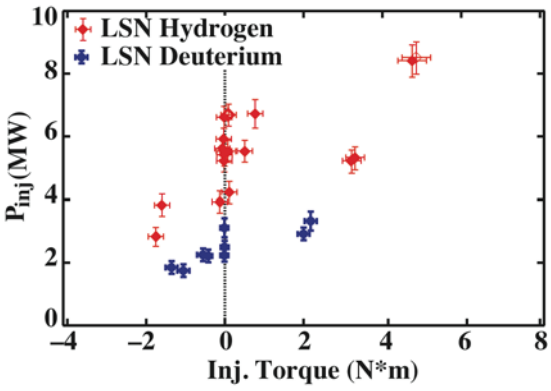

FIG. 5. Comparison of L-H threshold power vs neutral beam torque in hydrogen and deuterium plasmas.

well-matched dimensionless parameters showed that the density fluctuation amplitude was about twice as large in the hydrogen plasmas, consistent with the lower energy confinement time observed.

H-mode pedestal. ITER's fusion performance will depend strongly on the characteristics of the H-mode edge transport barrier, and recent work has led to significant advances in the capability to predict the barrier height. Previous work [8] has shown that edge stability is consistent with limits set by peeling-ballooning modes with toroidal mode numbers n~3–30. Recent experimental studies [9] using edge profile measurements with high spatial and temporal resolution, together with edge stability studies, motivate a simple model of the pedestal width in normalized poloidal flux: $\Delta(\psi_N) = 0.076\beta_{p,ped}^{1/2}$. Combining this width model with direct calculations of MHD peeling-ballooning stability (which predict the pedestal height as a function of the width) yields a new predictive model for both the pedestal height and width [10]. An experiment was then designed to test this model, yielding very good agreement across an order of magnitude in pedestal height (Fig. 6).

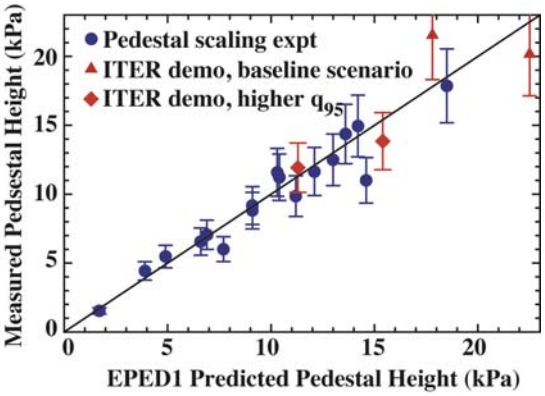

FIG. 6. Comparison of measured and predicted pedestal height for 21 DIII-D discharges, with varying triangularity, plasma current, and toroidal field.

Transport physics. Confident extrapolation of fusion performance from present devices to ITER requires understanding of the transport physics, and there has been significant progress in this area. Improvement of diagnostic instruments combined with the addition of synthetic diagnostics to gyrokinetic transport calculations has allowed unprecedented comparison of theory and experiment [11–13]. Simultaneous measurements of electron temperature fluctuations (with correlation ECE) and density fluctuations (with beam emission spectroscopy, Fig. 7) have been compared to GYRO code calcu-lations. The spectra predicted by synthetic CECE and BES diagnostics in the code are in very good agreement with the experimental data.

Quiescent H-mode. Quiescent H-mode (QH-mode) plasmas in DIII-D have now been achieved with co-injected neutral beams [14], where previously counter-injection was required. If it can be realized at ITER's operating parameters, the QH-mode represents a path to the desired conditions of a large edge pressure gradient but without the impulsive heat load generated by ELMs. The co-injected QH-mode has the expected features: ELM-free operation (for almost 1 s), constant density, and constant radiated power, with a continuous MHD mode that limits the pressure gradient at the edge. This edge harmonic oscillation (EHO) is believed to be a saturated kink-peeling mode located near the

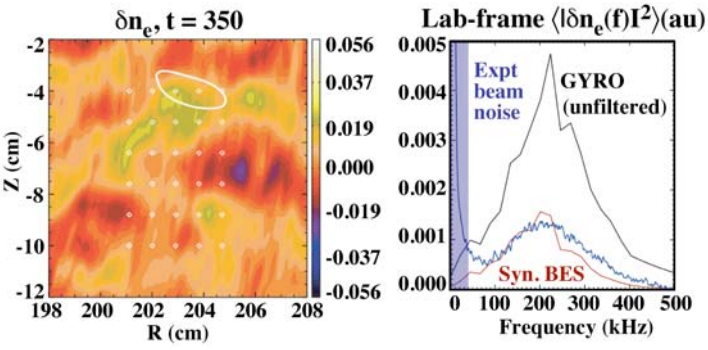

FIG. 7. Theory-experiment comparison of density fluctuation spectra measured with beam emission spectroscopy (BES), showing (a) experimental data, and (b) power spectrum in comparison to GYRO code predictions, including synthetic diagnostic calculations in GYRO.

edge of the plasma. A key element of these discharges is low density operation with divertor cryopumping, allowing rapid toroidal rotation. Although the co-injected QH-mode shows strong co-rotation across the entire profile, it has a strong rotational shear at the edge similar to that of the counter-injected case (Fig. 8), suggesting that rotational shear plays a key role in both cases. The existence of QH-mode with strong rotational shear for both co- and counter-rotation was predicted by theory [10].

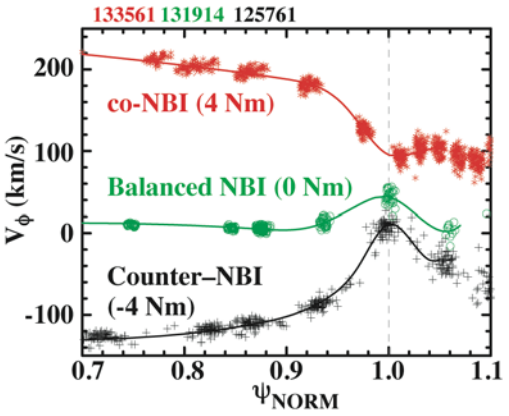

FIG. 8. Edge toroidal rotation profiles for cases with co (red), counter (black), and balanced (green) NBI. The co and counter cases are QH-mode.

Plasma rotation. A good understanding of the physics of plasma rotation is important for prediction of ITER's stability and confinement, but the physics of rotation is proving to be complex and subtle [15]. An "intrinsic" rotation is often seen in tokamak discharges without injected momentum. DIII-D experiments have determined that the anomalous torque associated with intrinsic rotation is also present in neutral beam-injected discharges. The anomalous torque is peaked near the edge of the plasma, and is consistent with a model of thermal ion orbit loss [16]. In addition, neoclassical theory predicts that non-resonant magnetic perturbations can create a torque of the form $T_{NRMF} \sim (V_\phi - V_\phi^0)$, where V_ϕ^0 is an "offset" velocity with a magnitude on the order of the ion diamagnetic drift but in the electron diamagnetic drift direction. This effect has been observed in high beta DIII-D plasmas [17]. As seen in Fig. 9, the application of an n=3 magnetic perturbation causes the rotation to approach an offset value of about -50 km/s; in cases where the initial velocity is near zero or slightly negative, this represents an *increase* in speed when the perturbation is applies. Such anomalous sources of torque may play an important role in ITER, where the neutral beam torque will be small.

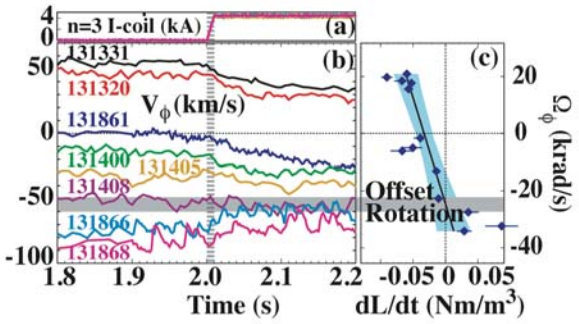

Fig. 9. (a) Applied n=3 magnetic perturbation, (b) the resulting evolution of the rotation velocity at ρ~0.8 for several different initial values of rotation, and (c) the inferred torque density as a function of the initial rotation.

Fast ions. New measurements in DIII-D are illuminating the physics of fast ion-driven instabilities and the associated fast ion transport [18]; scientific understanding and well-benchmarked transport and stability models are needed to predict the behavior of fusion alpha particles in ITER. Neutral beam injection into the discharge current ramp phase of reversed magnetic shear DIII-D plasmas [19] typically excites a variety of Alfvénic activity including toroidicity and ellipticity induced Alfvén eigenmodes (TAE and EAE) and reversed shear Alfvén eigenmodes (RSAE), revealed by fast interferometry [Fig. 10(a)], and fluctuation diagnostics such as electron cyclotron emission and beam emission spectroscopy. Fast-ion D_α (FIDA) spectroscopy shows that the central fast ion profile is flattened and the degree of flattening depends on Alfvén eigenmode amplitude. However, ion orbit calculations based on linear eigenfunctions from the NOVA code with measured mode amplitudes do not explain the observed fast ion transport [20]; multimode simulations with time-varying mode frequencies may be needed. Recent experiments have found that localized electron cyclotron

heating (ECH) applied near the shear reversal location can stabilize RSAE activity [Fig. 10(b,c)], resulting in significantly improved fast ion confinement [Fig. 10(d)]. FIDA measurements have also been used to measure fast wave absorption by energetic ions [21]. The recent capability for 2-D imaging of fast-ion D_α emission with a fast framing camera provides a potentially powerful new tool for study of fast ion transport.

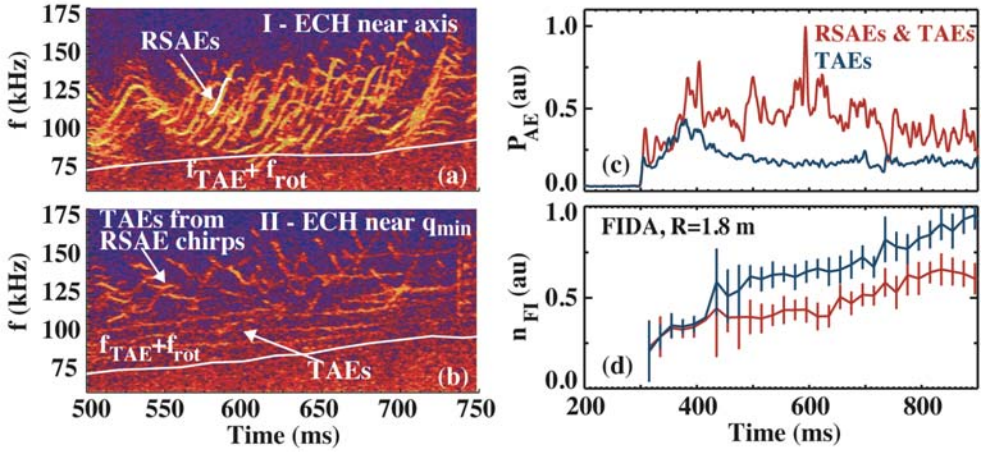

FIG. 10. Cross power spectra of vertical and radial interferometer chords in the frequency range of Alfvén instabilities (a) during ECH deposition near the magnetic axis, and (b) during ECH deposition near q_{min}. Also shown are the time evolution of (c) integrated power with ECH deposition near the axis (red) and near q_{min} (blue) and (d) the corresponding central fast ion density measured by the FIDA diagnostic.

4. Stability Control for Reliable Operation

Progress in DIII-D toward the understanding and control of MHD instabilities is contributing to the basis for stable and reliable operation in ITER, including suppression of ELMs with resonant magnetic perturbations, stabilization of neoclassical tearing modes (NTMs) with modulated electron cyclotron current drive, stabilization of resistive wall modes (RWMs) with direct feedback control, and understanding of the role of plasma rotation and error fields in the stability of both NTMs and RWMs.

Edge-localized modes. The suppression of ELM instabilities by resonant magnetic perturbations (RMP) offers a promising method to reduce the erosion of ITER's divertor targets. ELM suppression has now been demonstrated at ITER-like shape and collisionality [22] (Fig. 11). Recent DIII-D experiments and modeling [23] have provided key information for the assessment of new RMP coil options in ITER, using the Chirikov island overlap parameter as a guide.

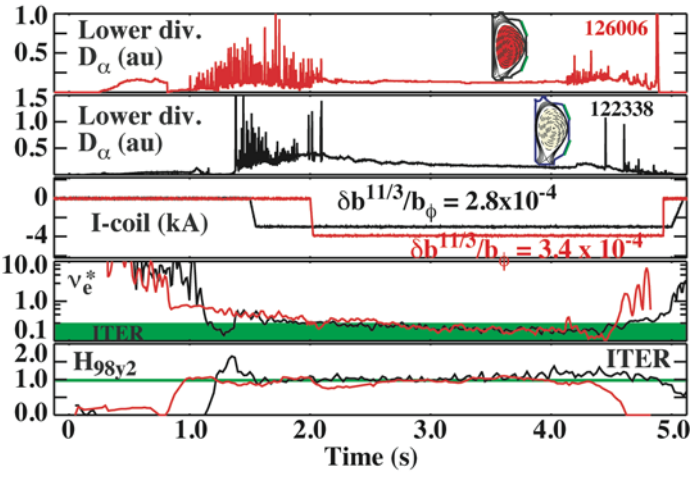

FIG. 11. Time evolution of discharges with ELM suppression, including divertor D_α emission, RMP coil current, pedestal collisionality (shading indicates ITER specification), and normalized energy confinement H_{98y2}. The cases shown are a high-triangularity ITER-similar shape (<δ>=0.53, red curves) and a lower-triangularity shape (<δ>=0.26, black curves).

In a comparison of coil configurations, ELM suppression was obtained with a single row of internal, small aperture, off-midplane coils (at larger current than with two such rows but with about the same RMP field strength) while suppression was not obtained with a single row of external, large aperture, on-midplane coils [24]; these results are consistent with the island overlap criterion. Injection of pellets for core fueling generates only small-amplitude bursts of edge recycling, which can be avoided by adjusting the RMP amplitude, suggesting that ELM suppression by RMP is compatible with pellet fueling. The ELM suppression is a result of enhanced particle transport at the edge; 3-D MHD simulation [25] and other work is in progress to determine the physical mechanism responsible, including a possible role of $E \times B$ convection cells. Initial experiments have begun to investigate ELM "pacing" by shallow pellet injection into the pedestal, and to investigate a recent, surprising discovery of ELM "pacing" by modulation of an n=3 RMP field.

Neoclassical tearing modes. Neoclassical tearing modes (and ELMs) are likely to be among the chief performance-limiting instabilities for ITER's baseline scenario. Studies with varying neutral beam torque have shown that the beta threshold for onset of 2/1 NTM instabilities decreases as the plasma rotation is reduced to ITER-relevant values (Fig. 12), consistent with a dependence of the effective Δ' stability parameter on rotational shear [26]. The 2/1 NTM onset also becomes much more sensitive to applied error fields in the low-torque, low-rotation cases. NTM suppression by continuous electron cyclotron current drive (ECCD) has been demonstrated previously; recent DIII-D experiments confirm expectations that the power requirement is reduced by modulation synchronized with the rotating island, using a novel technique to minimize modulation phase errors by detection of the island at the current drive location. DIII-D is contributing to an international effort to understand and model ECCD stabilization of NTMs in ITER [27]. High-quality images of the tearing mode structure using synchronous detection of visible bremsstrahlung emission agree well with an analytic model for the island structure [28], and will allow comparison of island dynamics to more detailed numerical models.

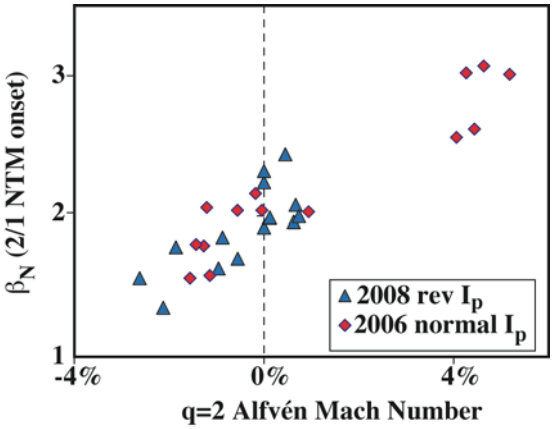

FIG. 12. Normalized beta at onset of m/n=2/1 NTM vs rotation velocity (normalized to Alfven velocity) at the q=2 surface, in an ITER-like single-null plasma.

Resistive wall modes. In high beta plasmas at or above the ideal MHD free-boundary stability limit, such as ITER's Q=5 steady-state scenario, resistive wall modes are stabilized at relatively slow plasma rotation, consistent with theoretical predictions that include kinetic effects [29]. However, high beta plasmas with low rotation are exceedingly sensitive to error fields and to excitation of RWMs by transient MHD events. DIII-D experiments [30] show sudden penetration of an applied n=1 magnetic perturbation followed by island formation. The critical amplitude of the applied perturbation decreases strongly above the no-wall stability limit as a result of the enhanced response of the marginally stable RWM, and the critical amplitude of the plasma response is independent of beta. With simultaneous use of ECCD to suppress tearing modes, and n=1 magnetic feedback to minimize static error fields and stabilize the plasma response to ELMs and fishbones, stability above the no-wall beta limit has been achieved at very low rotation [31] (Fig. 13).

5. Improving the Lifetime of Plasma-facing Components

DIII-D research is aimed at improving the lifetime of plasma-facing materials in fusion devices. Challenges that ITER will face include high transient heat flux and runaway electrons occurring during disruptions, as well as the time-averaged heat flux to the divertor. The proposed use of a carbon divertor during the deuterium phase of operation and possibly early in the D-T phase introduces the additional challenges of understanding the erosion, transport, and redeposition of carbon, and of recovering tritium retained in the carbon.

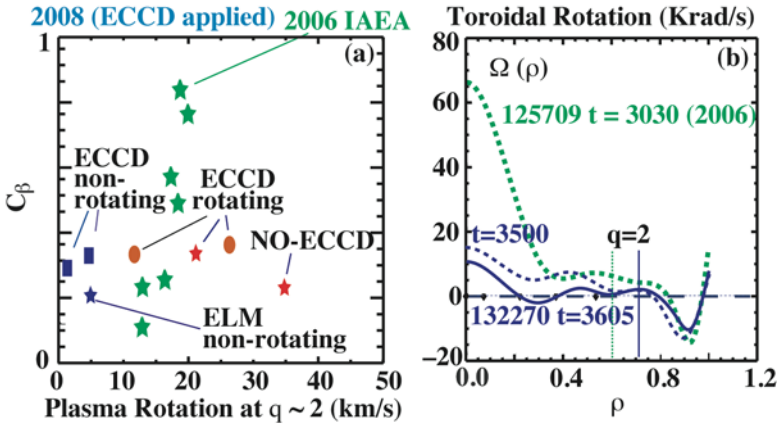

FIG. 13. RWM stability at low rotation. (a) C_β, the beta value scaled such that C_β=0 at the no-wall limit and C_β=1 at the ideal-wall limit, vs plasma rotation at the q=2 surface. Squares indicate cases with non-rotating modes, circles indicate cases with rotating modes (most likely NTM), and stars indicate cases without RWM feedback. Included are recent cases with ECCD for suppression of NTMs, and 2006 data without ECCD (green squares). (b) Rotation profile at the mode onset in a low-rotation ECCD-stabilized case, compared to a 2006 case without ECCD.

Disruption mitigation. Mitigation of disruptions by rapid injection of various gas species has successfully provided radiative dissipation of the plasma thermal energy and fast plasma current shutdown, reducing thermal loads and vertical forces on the vacuum vessel [32]. However, the $\geq 10^{22}$ m^{-3} electron density required for collisional suppression of a runaway electron avalanche (the "Rosenbluth density") is about an order of magnitude larger than densities achieved to date, and remains a challenge. Experiments [33] and 3D nonlinear modeling [34] show that MHD instabilities are important in mixing the impurity gas into the plasma core, and DIII-D experiments using a fast rise-time multi-valve system have shown the importance of delivering the gas to the plasma before the end of the thermal quench. The latter condition favors light gas species, high throughput, and delivery systems close to the plasma [35]. Assimilation fractions (fraction of injected atoms that become ionized) up to 40% are found with helium injection, as seen in Fig. 14. H_2 and D_2 show somewhat smaller assimilation, but all of these low-Z species exhibit a favorable increase of the assimilation fraction with the quantity of injected gas. A mixture of D_2+2% Ne also shows promise. Alternative methods for rapid, high-density impurity injection such as low-Z pellets are being explored.

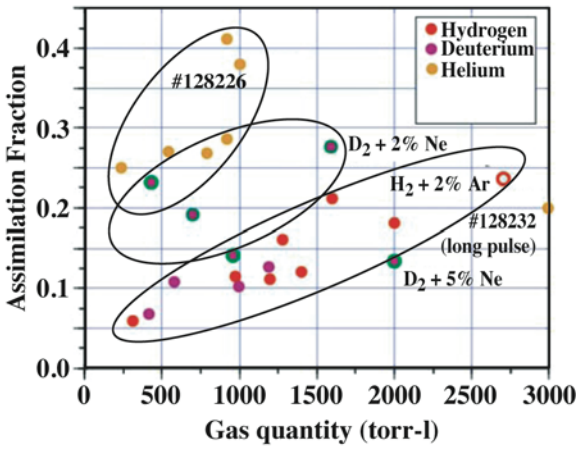

FIG. 14. Assimilation fraction ($N_{ionized}$/$N_{injected}$) for low-Z species: H_2, D_2, He, and dilute mixtures of high-Z species (Ne and Ar). Also shown is one "long-pulse" helium case where much of the gas arrived at the plasma after the start of the current quench.

Radiative divertor. One way to ameliorate the problem of divertor heating is to introduce "seed" impurities (e.g. argon) directly into the divertor, where they can radiate a significant fraction of the plasma-conducted power before the plasma particles reach the divertor

surface. Leakage of the impurity into the main plasma can be minimized by maintaining a strong flow of deuterium ions into the divertor through upstream deuterium gas puffing and active particle exhaust at the divertor targets. DIII-D experiments show that both the accumulation of argon inside the main plasma and the removal of argon from the divertor are sensitive to the divertor topology and the ion $B \times \nabla B$ drift direction [36, 37]. With argon injection into the private flux region of the upper divertor, the rate of argon accumulation in the core was found to be as much as a factor of 3 smaller with the $B \times \nabla B$ drift away from the divertor (Fig. 15), and the rate of argon removal was a factor of 2–3 greater, in comparison to the case with the drift toward the divertor. Double-null divertor configurations showed stronger argon accumulation than single-null, for the same direction of $B \times \nabla B$ drift. Modeling with UEDGE, using a new capability to model drifts in a balanced double null configuration, reproduces some of the key features of the experiments and indicates that the direction of the $E_r \times B$ drift near the x-point may play a key role. Experiments show that the radiative divertor is compatible with hybrid scenario operation.

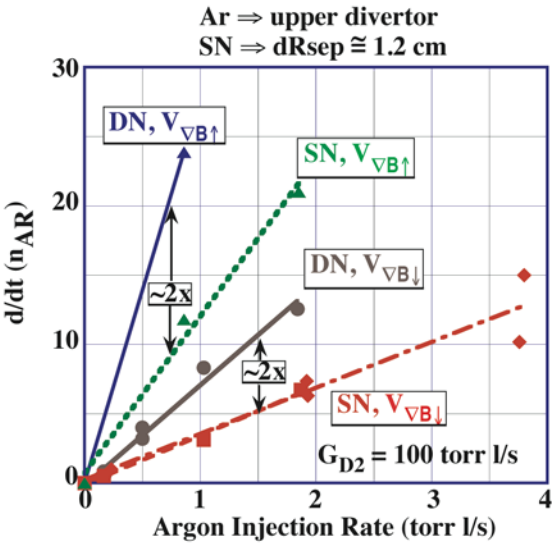

FIG. 15. Rate of core argon accumulation vs argon injection rate into the upper divertor, for four cases: drift upward or downward, and double-null or upper single-null plasmas.

Carbon walls and tritium retention. Carbon has many advantages as a plasma-facing material, but retention of tritium is a critical issue for its use in ITER. DIII-D research is investigating the physics of the transport and co-deposition of carbon and hydrogenic fuel, and methods for removing the co-deposits. Spectroscopic measurements show that the poloidal flow of singly ionized carbon in the scrape-off layer is decoupled from the core plasma's rotation, but is consistent with an $E_r \times B$ drift due to a radial electric field in the scrape-off layer [38]. Fast camera imaging now provides information on the quantity and motion of dust particles in DIII-D discharges [39]. Experiments have shown that co-deposition of carbon and deuterium is reduced on heated surfaces [40] and local gas injection has been successful in minimizing co-deposition on diagnostics mirror samples. Laboratory tests of samples taken from DIII-D have shown that thermal oxidation is effective at removing carbon co-deposits; tokamak co-deposits have open structures and erode 2–3 orders of magnitude faster than the more dense lab-produced films. Extensive testing has been carried out to determine the effects of oxygen (or air) baking on the various materials found in the DIII-D vacuum vessel, with the ultimate goal of an in situ test of co-deposit removal.

6. Summary and Future Research Directions

We have summarized recent DIII-D research in support of ITER, including the development of operating scenarios for projections of fusion performance and tests of plasma control; fusion science studies that provide the basis for prediction and improvement of ITER's performance; improvement of ITER's reliability through control of instabilities; and development of the means to control and mitigate the plasma's interaction with surrounding materials.

Future DIII-D research will continue to address scientific and technical issues for ITER. New hardware capabilities are anticipated in the next several years to enable this research,

including extension of the heating systems' pulse lengths, high-density impurity delivery systems for disruption mitigation, and operation with heated walls and divertor targets for reduction of hydrogenic species co-deposition. A new set of RMP coils will enable further study of the physics of the stochastic edge and ELM control.

The planned modification of a neutral beam line for injection with variable vertical angle will allow studies of off-axis neutral beam current drive, as anticipated in ITER's steady-state scenarios. Recent experiments have validated models of off-axis current drive [41], using DIII-D's existing midplane injectors with small, vertically shifted plasmas. As shown in Fig. 16, the current drive efficiency is sensitive to the beam's alignment with the local magnetic field. Detailed transport modeling [42] predicts that, in full-sized DIII-D plasmas, a vertically tilted beam line will provide up to 200 kA of current drive centered at mid-radius. Such experiments will support the use of off-axis NBI in ITER's steady-state scenarios.

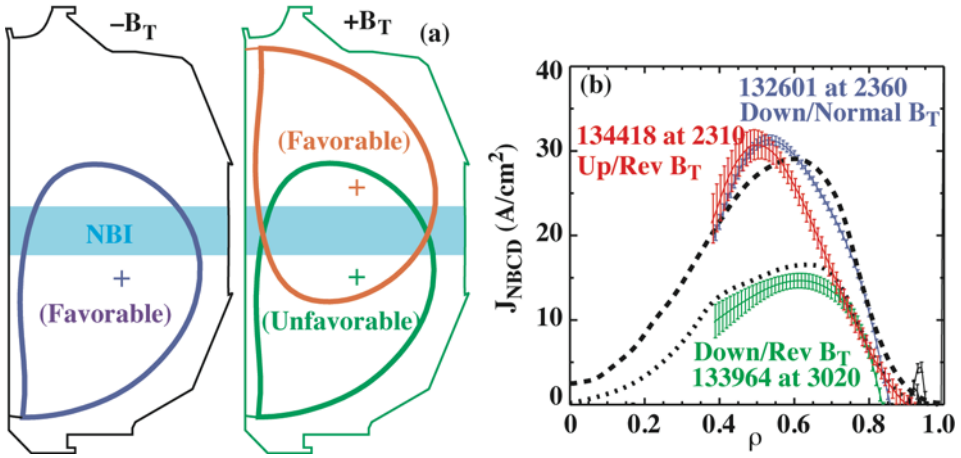

FIG. 16. (a) Small, vertically shifted plasmas allow tests of off-axis beam injection. (b) Experimentally measured neutral beam current drive (vertical bars) is in good agreement with transport model predictions (dotted curves). Current drive with unfavorable magnetic field pitch (green) is about half that obtained with favorable pitch (red and blue).

Acknowledgments

This work was supported by the US Department of Energy under DE-FC02-04ER54698.

References

[1] DOYLE, E.J., *et al.,* this conference, EX/1-3.
[2] YUSHMANOV, P.N., et al., Nucl. Fusion **30**, 1999 (1990).
[3] PETTY, C.C., *et al.,* this conference, EX/1-4Rb.
[4] HUMPHREYS, D.A., *et al.,* this conference, IT/2-4Rb.
[5] JACKSON, G.L., *et al.,* this conference, IT/P7-2.
[6] FERRON, J.R., *et al.,* this conference, EX/P4-27.
[7] McKEE, G.R., *et al.,* this conference, EX/10-1.
[8] SNYDER, P.B., *et al.,* Nucl. Fusion **47**, 961 (2007).
[9] GROEBNER, R.J., *et al.,* this conference, EX/P3-5.
[10] SNYDER, P.B., *et al.,* this conference, IT/P6-14.
[11] WHITE, A.E., *et al.,* Phys. Plasmas **15**, 056116 (2008).
[12] SCHMITZ, L., *et al.,* this conference, EX/P5-35.
[13] HOLLAND, C., *et al.,* this conference, TH/8-1.
[14] BURRELL, K.H., *et al.,* this conference, EX/8-4.
[15] SOLOMON, W.M., *et al.,* this conference, EX/3-4.
[16] deGRASSIE, J.S., *et al.,* this conference, EX/P5-2.

[17] GAROFALO, A.M., *et al.,* "Observation of plasma rotation driven by static non-axisymmetric magnetic fields in a tokamak," to be published in Phys. Rev. Lett. (2008).
[18] VAN ZEELAND, M.A., *et al.,* this conference, EX/6-2.
[19] NAZIKIAN, R., *et al.,* Phys. Plasmas **15**, 056107 (2008).
[20] HEIDBRINK, W.W., *et al.,* Phys. Rev. Lett. **99**, 245002 (2007).
[21] PINSKER, R.I., *et al.,* this conference, EX/P6-24.
[22] EVANS, T.E., *et al.,* this conference, EX/4-1.
[23] FENSTERMACHER, M.E., *et al.,* Phys. Plasmas **15**, 056122 (2008).
[24] FENSTERMACHER, M.E, *et al.,* "Suppression of Type-I ELMs using a single toroidal row of magnetic field perturbation coils in DIII-D," submitted to Nucl. Fusion (2008).
[25] IZZO, V.A., *et al.,* this conference, TH/P4-19.
[26] BUTTERY, R.J., *et al.,* Phys. Plasmas **15**, 056115 (2008); this conference, IT/P6-8.
[27] LA HAYE, R.J., *et al.*, this conference, IT/P6-9.
[28] VAN ZEELAND, M.A., *et al.,* Nucl. Fusion **48**, 092002 (2008).
[29] REIMERDES, H., *et al.,* Plasma Phys. Control. Fusion **49**, B349 (2007).
[30] REIMERDES, H., *et al.,* this conference, EX/5-3Ra.
[31] OKABAYASHI, M., *et al.,* this conference, EX/P9-5.
[32] GRANETZ, R.S., *et al.,* Nucl. Fusion **47**, 1086 (2007).
[33] HOLLMANN, E.M., *et al.,* "Measurements of injected impurity assimilation during massive gas injection experiments in DIII-D," to be published in Nucl. Fusion (2008).
[34] IZZO, V.A., *et al.,* Phys. Plasmas **15**, 056109 (2008).
[35] WESLEY, J.C., *et al.,* this conference, EX/7-3Rb.
[36] PETRIE, T.W., *et al.,* Nucl. Fusion **48**, 045010 (2008).
[37] PETRIE, T.W., *et al.,* this conference, EX/P4-21.
[38] GROTH, M., *et al.,* this conference, EX/P4-19.
[39] RUDAKOV, D.L., *et al.,* this conference, EX/9-3.
[40] LITNOVSKY, A., *et al.,* Fusion Eng. and Design **83**, 79 (2008).
[41] MURAKAMI, M., *et al.,* this conference, TH/P3-1.
[42] MURAKAMI, M., *et al.,* to be published in Fusion Sci. Tech. (2008).

APPENDIX: THE DIII–D TEAM

S.S. Abdullaev,[1] G. Abla,[2] T. Abrams,[3] M.P. Aldan,[4] N.B. Alexander,[2] S.L. Allen,[5] D. Anastasi,[2] P.M. Anderson,[2] M.E. Austin,[6] F.W. Baity,[7] J.P. , Bakalarski,[2] T. Barber,[7] V. Basiuk,[8] E.M. Bass,[9] G. Bateman,[10] C.B. Baxi,[2] L.R. Baylor,[7] M. Becoulet,[8] E.A. Belli,[9] H.L. Berk,[6] J.W. Berkery,[11] L.A. Berry,[7] M. Beurskens,[12] J.M. Bialek,[11] J.A. Boedo,[13] I.N. Bogatu,[14] R.L. Boivin,[2] A.H. Boozer,[11] R.V. Bravenec,[6] B.D. Bray,[2] D.P. Brennan,[15] S. Brezinsek,[1] N.H. Brooks,[2] L.C. Brown,[2] C.D. Brunkhorst,[16] R.V. Budny,[16] R. Bulmer,[5] K.H. Burrell,[2] R.J. Buttery,[12] J.D. Callen,[17] R.W. Callis,[2] G.L. Campbell,[2] J.M. Candy,[2] J. Canik,[7] T.N. Carlstrom,[2] T.A. Carter,[18] R. Carver,[19] W.P. Cary,[2] A. Casati,[8] T.A. Casper,[5] A. Castano,[16] M. Cengher,[2] C.D. Challis,[12] F.R. Chamberlain,[2] V.S. Chan,[2] M.S. Chance,[16] S. Chang,[20] S.N. Chen,[3] R. Chipman,[21] H.K. Chiu,[2] M. Choi,[2] M.S. Chu,[2] R.J. Colchin,[7] A.J. Cole,[17] G. Colyer,[12] S.K. Combs,[7] N. Commaux,[7] WA, Cooper,[22] D. Coster,[23] J. Dalessio,[10] J.W. Davis,[24] J.C. DeBoo,[2] J.S. deGrassie,[2] S.J. DePasquale,[16] T.M. Deterly,[2] J.L. Doane,[2] J. Dorris,[3] E.J. Doyle,[18] N. Eidietis,[9] D. Elder,[24] R. Ellis,[5] R.A. Ellis,[16] R.F. Ellis,[25] T.E. Evans,[2] M. Fahey,[7] R. Feder,[16] D. Fehling,[7] E.A. Feibush,[16] Y. Feng,[26] M.E. Fenstermacher,[5] M. Ferrara,[3] J.R. Ferron,[2] K.H. Finken,[1] D.K. Finkenthal,[27] R.K. Fisher,[2] D. Fitzpatrick,[24] B.W.N. Flanagan,[2] S.M. Flanagan,[15] R.J. Fonck,[17] J.M. Foster,[28] E. Fredd,[16] R. Freeman,[29] H.G. Frerichs,[1] R.K. Friend,[30] Z. Friis,[31] G.Y. Fu,[16] Q. Gao,[32] A.M. Garofalo,[2] K.W. Gentle,[6] A. Geraud,[8] P. Gohil,[2] N.N. Gorelenkov,[16] I.A. Gorelov,[2] P.A. Gourdain,[18] K.L. Greene,[2] C.M. Greenfield,[2] N.L. Greenough,[16] R.J. Groebner,[2] M. Groth,[5] H.J. Grunloh,[2] M.F. Gu,[5] W. Guo,[33] A.A. Haasz,[24] S.H. Hahn,[34] F.D. Halpern,[10] J. Hansink,[2] J. Harhausen,[23] J.H. Harris,[35] P. Hartigan,[19] D. Harting,[1] R.W. Harvey,[36] N.C. Hawkes,[12] R.J. Hawryluk,[16] C. Hegna,[17] W.W. Heidbrink,[37] M.F. Heyn,[38] D.N. Hill,[5] D.L. Hillis,[7] J. Hillscheim,[18] J.K. Hobirk,[39] C.T. Holcomb,[5] C. Holland,[13] E.M. Hollmann,[13] K.L. Holtrop,[2] R.M. Hong,[2] L. Horton,[23] J.C. Hosea,[16] C.L. Hsieh,[2] A.E. Hubbard,[3] A. Huber,[1] B. Hudson,[9] J. Hughes,[3] D.A. Humphreys,[2] I.H. Hutchinson,[3] P. Huynh,[2] G.T.A. Huysmans,[8] A.W. Hyatt,[2] S. Ide,[40] F. Imbeaux,[8] Y. In,[14] K. Indireshkumar,[16] A. Isayama,[40] R.C. Isler,[7] I.B. Ivanov,[38] V.A. Izzo,[13] G.L. Jackson,[2] A.M. Jacobs,[41] E.F. Jaeger,[7] M. Jakubowski,[1] A.N. James,[13] R.J. Jayakumar,[5] Y.M. Jeon,[9] T.C. Jernigan,[7] E.H. Joffrin,[8] P. Johnson,[42] R.D. Johnson,[2] I. Joseph,[5] K. Kajiwara,[9] A. Kallenbach,[23] Y. Kamada,[40] D.H. Kaplan,[2] S.V. Kasilov,[38] A. Kasugai,[40] K.M. Keith,[2] A.G. Kellman,[2] D.H. Kellman,[2] J. Kim,[14] J.S. Kim,[14] J.E. Kinsey,[2] C. Konz,[26] M. Kotschenreuther,[6] G.J. Kramer,[16] S.I. Krasheninnikov,[13] A.H. Kritz,[10] R.J. La Haye,[2] B. Labombard,[3] M.J. Lanctot,[11] L.L. Lao,[2] C.J. Lasnier,[5] E.A. Lazarus,[7] R.L. Lee,[2] X. Lee,[2] M. Lehnen,[1] A.W. Leonard,[2] J.A. Leuer,[2] F.M. Levinton,[43] J. Li,[33] L. Li,[33] B. Lipschultz,[3] J. Lister,[22] Y.Q. Litnovsky,[1] A. Liu,[2] D. Liu,[37] C. Liu,[12] L.L. Lodestro,[5] N. Logan,[44] J. Lohr,[2] T.C. Luce,[2] C.A. Ludescher-Furth,[16] Y. Luo,[37] C.F. Maggi,[23] S.M. Mahajan,[1] S.B. Mahar,[17] M.A. Mahdavi,[45] J. Mailloux,[12] R. Maingi,[7] M.A. Makowski,[5] M.E. Maraschek,[23] M. Marrelli,[46] L. Martin,[46] P. Martin,[47] P.S. Mauzey,[2] D. Mazon,[8] S. McClain,[21] D.C. McCune,[16] W.L. McDaniel,[2] B.B. McHarg,[2] G.R. McKee,[17] A.G. McLean,[24] A. Meyer,[5] D. Mikkelsen,[16] D.C. Miller,[2] D.W. Miller,[16] C.P. Moeller,[2] P. Monier-Garbet,[8] S. Mordijck,[13] K. Morris,[5] R.A. Moyer,[13] Y.R. Mu,[24] S. Müller,[13] M. Murakami,[7] C.J. Murphy,[2] C. Muscatello,[37] A. Nagy,[16] E. Nardon,[8] M.F.A. Nave,[48] G.A. Navratil,[11] R. Nazikian,[16] X.V. Nguyen,[18] A. Nikroo,[2] S. Noraky,[2] R.E. Nygren,[49] R.C. O'Neill,[2] Y. Oda,[40] Y.K. Oh,[50] M. Okabayashi,[16] R.A. Olstad,[2] D. Orlov,[13] T.H. Osborne,[2] Y. Ou,[10] L.W. Owens,[7] N, Oyama,[40] N.A. Pablant,[13] J. Palmer,[19] C. Pan ,[33] A.Y. Pankin,[10] J.K. Park,[20] G. Park,[7] J.M. Park,[16] C.T. Parker,[2] P.B. Parks,[2] C.J. Pawley,[2] L.D. Pearlstein,[5] W.A. Peebles,[18] B. Pegourie,[8] B.G. Penaflor,[2] P.I. Petersen,[2] T.W. Petrie,[2] C.C. Petty,[2] N.Q. Pham,[2] V. Philipps,[1] A.Yu. Pigarov,[13] D.A. Piglowski,[2] R.I. Pinsker,[2] P.A. Politzer,[2] D.M. Ponce,[2] M. Porkolab,[3] G.D. Porter,[5] A. Pospieszezyk,[1] R. Prater,[2] J. Qian,[33] T. Rafiq,[10] D. Raju,[51] M. Ramm,[52] L.E. Randerson,[16] H. Reimerdes,[11] D. Reiser,[1] Q. Ren,[33] M.E. Rensink,[5] G. Rewoldt,[16] T.L. Rhodes,[18] H. Rinderkhecht,[16] T.D. Rognlien,[5] P.A. Rosen ,[28] M. Rosenberg,[13] J.C. Rost,[3] R. Rubilar,[17] D.L. Rudakov,[13] A. Runov,[26] E. Ruskov,[37] P.M. Ryan,[7] D. Ryutov,[5] S. Saarelma,[12] S.A. Sabbagh,[11] G. Saibene,[23] Y. Sakamoto,[40] U. Samm,[1] B.S. Sammuli,[2] F. Sartori,[12] R.I. Savercool,[2] M.J. Schaffer,[2] D.P. Schissel,[2] D.J. Schlossberg,[17] O. Schmitz,[1] L. Schmitz,[18] D.G. Schneider,[8] E. Schuster,[10] J.T. Scoville,[2] S. Sears,[53] A. Sen,[51] M.W. Shafer,[17] J.P. Sharpe,[54] T.Y. Sheffield,[55] J.Y. Shiriashi,[9] K.C. Shoolbred,[2] R.D. , Sips,[23] A.C.C. Smirnov,[56] A.P. Smirnov,[13] J.P. Smith,[2] P.B. Snyder,[2] W.M. Solomon,[16] R. Srinivason,[51] H.E. St. John,[2] W.M. Stacey,[31], G.M. Staebler,[2] R.D. Stambaugh,[2] P.C. Stangeby,[24] C. Stemprok,[2] N.C. Stone,[47] E.J. Strait,[2] R.W. Street,[2] J.D. Stromsoe,[13] T. Suzuki,[40] W.S. Sweet,[2] H. Takahashi,[16] D.A. Taussig,[2] P.L. Taylor,[2] T.S. Taylor,[2] W. Terry,[3] D.M. Thomas,[2] M. Tillack,[13] M. Tokar,[1] J.F. Tooker,[2] Y. Treutterer,[23] J. Tucci,[57] F. Turco,[9] A.D. Turnbull,[2] G.R. Tynan,[13] M. Umansky,[5] K. Umstadter,[13] E.A. Unglaub,[58], W. Unterberg,[1] B. Unterberg,[9] H. Urano,[40] P. Valanju,[6] E. Valeo,[16] M.A. VanZeeland,[2] S. Visser,[2] G. Vlad,[59] F. Volpe,[23] J. Von Der Lindon,[60] M.R. Wade,[2] M.L. Walker,[2] R.E. Waltz,[2] W.R. Wampler,[49] B. Wan,[33] S.J. Wang,[33] A. Wang,[32] G. Wang,[18] J.G. Watkins,[49] A.S. Welander,[2] J.C. Wesley,[2] W.P. West,[2] B. White,[16] R. White,[18] D.G. Whyte,[3] R.J.R. Williams,[28] H.R. Wilson,[61] A. Wingen,[62] M. Wischmeier,[23] R. Wolf,[26] S.M. Wolfe,[3] C.P.C. Wong,[2] N. Wong,[2] S.K. Wong,[5] W. Wu,[2] B. Xiao,[33] H.W. Xu,[2] X. Xu,[5] S. Yang,[10] H.H. Yip,[2] Y.S. Yoon,[63] D. Young,[64] J.H. Yu,[13] Q. Yuan,[33] H. Yuh,[43] L. Zeng,[18] Y. Zhu[37]

AFFILIATIONS

[1]EURATOM-FZ Julich
[2]General Atomics
[3]Massachusets Institute of Technology
[4]University of California, Berkeley
[5]Lawrence Livermore National Laboratory
[6]University of Texas
[7]Oak Ridge National Laboratory
[8]CEA Cardache Euratom Association
[9]LeHigh University
[10]Oak Ridge Institute of Science Education
[11]Columbia University
[12]UKAEA Fusion Culham Science Center
[13]University of California, San Diego
[14]FARTECH, Inc.
[15]University of Tulsa
[16]Princeton Plasma Physics Laboratory
[17]University of Wisconsin
[18]University of California, Los Angeles
[19]Rice University
[20]New York University
[21]University of Arizona
[22]CRPP-EPFL-Lausanne
[23]Max Plank Institut für Plasmaphysik, Garching
[24]University Toronto
[25]University Maryland
[26]Max Plank -Griefswald
[27]Palomar College
[28]AWE Communications
[29]Ohio State University
[30]Washington & Lee University
[31]Georgia Institute of Technology
[32]SWIPP, Chengdu, China
[33]ASIPP-Hefei
[34]National Fusion Research Center, Korea
[35]Australian National University
[36]CompX
[37]University of California, Irvine
[38]Euratom-ÖAW ITP Graz, Austria
[39]Max Plank Institute
[40]Japan Atomic Energy Agency (JAEA)
[41]Hendrix College
[42]Butler University
[43]Nova Photonics
[44]Brown University
[45]ALITRON
[46]Consorzio RFX
[47]Cornell University
[48]EURATOM Lisbon
[49]Sandia National Laboratory
[50]National Fusion Research Institute, Korea
[51]Institure for Plasma Research, India
[52]Stanford University
[53]West Virginia University
[54]Idaho National Laboratory
[55]TCU
[56]Moscow State University
[57]Notre Dame University
[58]Colorado School of Mines
[59]ENEA-Frascati
[60]University of Pennsylvania
[61]University of York
[62]University of Düsseldorf
[63]Korea Atomic Energy Research Institute